IEEE Access
Multidisciplinary | Rapid Review | Open Access Journal

Received February 27, 2018, accepted April 2, 2018, date of publication April 10, 2018, date of current version May 16, 2018.

Digital Object Identifier 10.1109/ACCESS.2018.2825363

A Frequency Regulation Strategy for Wind Power Based on Limited Over-Speed De-Loading Curve Partitioning

XU ZHANG[1], (Member, IEEE), XIAOBING ZHA[2], SHUAI YUE[1], (Student Member, IEEE), AND YUNLONG CHEN[1]

[1]School of Electrical and Electronic Engineering, North China Electric Power University, Beijing 102206, China
[2]State Grid Jiangsu Electric Power Co., Ltd., Maintenance Division Headquarters, Nanjing 211102, China

Corresponding author: Xu Zhang (zxtemper@163.com)

This work was supported in part by the National Key Research and Development Program of China under Grant 2017YFB0902600 and in part by the Fundamental Research Funds for the Central Universities under Grant 2015MS24.

ABSTRACT Over the past decade, wind power has rapidly developed, bringing great challenges to power system frequency control. To enable wind turbines (WTs) to operate with independent frequency regulation similar to that of synchronous generators, the development of strategies for wind power frequency regulation has received increasing attention. Here, a frequency regulation strategy by wind power based on limited over-speed de-loading curve partitioning is proposed. On the basis of the rotor kinetic energy control, the relationship between the de-loading capacity of over-speed control and wind speed is studied. Combined with the data fitting, the limited over-speed de-loading level curve of the WT is obtained to partition over-speed de-loading and pitch de-loading; this approach maximizes the use of over-speed de-loading and enhances the frequency regulation capacity of the WT. Finally, based on DIgSILENT/PowerFactory software, a four-machine two-zone power system model and an IEEE-39 bus system are built, and the control effects of this control strategy under different penetration levels, different wind speeds and different de-loading levels are compared and analyzed. The simulation results show that the control strategy can effectively improve the frequency response capability of wind power systems.

INDEX TERMS Wind power frequency regulation, de-loading partitioning, rotor kinetic energy control, over-speed control, pitch control, limited over-speed de-loading curve.

I. INTRODUCTION

The wind power grid capacity in the global market was more than 54.6 million kilowatts in 2016, and the total wind power grid capacity reached 486.7 million kilowatts, revealing a rapid development of wind power worldwide. A large number of wind turbines (WTs), represented by doubly fed induction generators (DFIGs), have brought great challenges to the power system frequency control. On the one hand, the DFIG decouples its system through the converter connecting to the system, which cannot take the initiative to respond to frequency changes of the power system. On the other hand, the DFIG generally runs at maximum power point tracking (MPPT), which cannot provide active standby for the system and participate in system frequency regulation [1], [2].

To provide WTs with frequency response capability, a control loop is introduced appropriately into WTs in [3], [4]; this control loop allows WTs to respond to the change of system frequency by using the rotational kinetic energy hidden inside the rotor and enhances the inertial response capability of the system. On the basis of this approach, the parameters of the proposed control strategy were optimized to improve the adaptability of the rotor kinetic energy control in [5]–[7]; however, the controllable kinetic energy in the rotor is limited, and thus, the regulating ability is insufficient. Because WTs cannot provide active standby, rotor over-speed control and pitch control (PC) were respectively adopted by [8], [9] to serve as a reserve for system frequency regulation. In [10]–[12], considering equipment outside of the WT, energy storage equipment was used to help the WTs to participate in system frequency regulation; however, this approach is not conducive to the economic operation of wind farms because the additional energy storage system requires

additional equipment. In [13], according to the wind conditions, the WT operating area was divided into high, medium and low wind speed areas. The PC was used in the high wind speed area, OSC and PC were used in the medium wind speed zone, and OSC was used in the low wind speed area, which has a certain frequency regulation advantage. In [14], a wind power frequency regulation strategy of over-speed reduction control combined with inertial control was proposed that can effectively improve the system frequency regulation ability; however, it cannot be applied to the high wind speed condition because of the limitation of over-speeding de-loading capacity. In [15], an online de-loading instruction model was proposed combining rotor kinetic energy control (RKC) and PC, which decouples the pitch angle and power control to respond quickly to wind speed variation; however, this system relies mainly on PC, which exacerbates the wear of mechanical parts. To suppress the power drop caused by the RKC, in [16], a control strategy adopting RKC and OSC when the wind speed is lower than the rated wind speed and adopting the RKC and PC when the wind speed is higher than the rated wind speed was proposed; this approach can suppress power drop effectively. In [17], a control method was proposed that switched the operation mode (SOM) of WTs. This method mainly aids in the system frequency regulation under different wind speed conditions through the overproduction control, the de-loading control and the overload control.

Although the above-described control strategies have certain advantages, most of the strategies use a method of fixed partitioning to achieve over-speed de-loading and pitch de-loading control switching. Thus, the application range of the over-speed control is limited by the wind speed and the de-loading level. In addition, most of the above-described control strategies use a fixed partitioning method to switch over-speed control and pitch control. The scope of speed control is determined by the wind speed and the de-loading level. Different de-loading levels will change the running characteristic curve of the WT, and the application scope of the over-speed control will change. The use of fixed partitioning cannot adapt to this change and cannot fully utilize the frequency potential of the WT.

In this paper, a wind power frequency regulation control strategy based on limited over-speed de-loading curve partitioning is proposed. This paper analyzes the frequency regulation ability of OSC and PC theoretically, quantifies the application range of OSC and deduces and fits the over-speed limited de-loading curve. Based on RKC, the partition control is implemented according to the limited over-speed de-loading curve. The strategy can adjust the demarcation point according to the de-loading level, take full advantage of the rapid response advantage of rotor kinetic energy control (RKC), improve the inertia of WTs in the case of low wind speed and, to a certain extent, avoid mechanical wear caused by frequent pitch. The simulation results show that the proposed strategy can provide better frequency support for a power system under complex conditions.

The remainder of this paper is organized as follows. Section II introduces the current frequency regulation control method via DFIGs. Section III explains the partition method based on the limited over-speed de-loading curve, and Section IV discusses the joint control based on limited over-speed de-loading curve partitioning. Section V presents three cases in which the proposed method is applied to a real frequency regulation scenario. Finally, Section VI provides the main conclusions of this paper.

II. FREQUENCY REGULATION CONTROL METHOD WITH A DFIG

According to the theory of aerodynamics, the output power of the DFIG can be expressed as follows:

$$\begin{cases} P = \dfrac{1}{2}\rho C_p(\lambda, \beta)\pi R^2 V^3 \\ C_p(\lambda, \beta) = 0.22(\dfrac{116}{\lambda_i} - 0.4\beta - 5)e^{\dfrac{-12.5}{\lambda_i}} \\ \dfrac{1}{\lambda_i} = \dfrac{1}{\lambda + 0.08\beta} - \dfrac{0.035}{\beta^3 + 1} \end{cases} \tag{1}$$

In (1), $\lambda = \omega R/V$ is the tip speed ratio, β is the pitch angle, ω is the rotating speed, R represents the blade radius, V is the wind speed, ρ is the air density, C_p is the wind energy utilization factor, and λ_i is intermediate variable [18]. The output of a WT is mainly related to wind speed, rotating speed and pitch angle. Because the wind speed is too random and fluctuating to control, the power system frequency is regulated by wind power mainly through the control of rotor speed and pitch angle to control the output to respond to the frequency change. The main control strategies are RSC and de-loading control (DLC).

A. ROTOR KINETIC ENERGY CONTROL

The principle of RKC is that when the system frequency changes, RKC takes advantage of the exchange of the rotor kinetic energy in WT rotors and the electromagnetic power of WT to maintain system frequency stability.

The total kinetic energy E_k of a WT rotor is as follows:

$$E_k = \frac{1}{2}J\omega^2 \tag{2}$$

In (2), J is the mechanical moment of inertia of the WT, and ω is the WT's speed. After the WT speed changes, the conversion energy between kinetic energy and electromagnetic power is as follows:

$$\Delta E = \frac{1}{2}J(\omega_2^2 - \omega_1^2) \tag{3}$$

In (3), ω_1 and ω_2 are the rotor speed before and after control, respectively. To establish the connection between the output and the frequency of the WT, a ΔP signal related to the system frequency deviation and the rate of change is introduced into the active power control link of the WT, as shown in the following equation (4):

$$\Delta P = -K_{df}\frac{df}{dt} - K_{pf}\Delta f \tag{4}$$

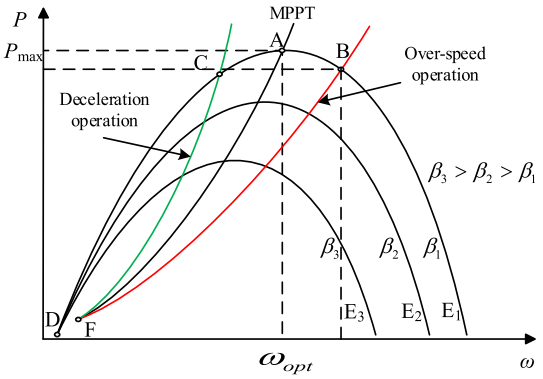

FIGURE 1. DFIG de-loading operation schematic.

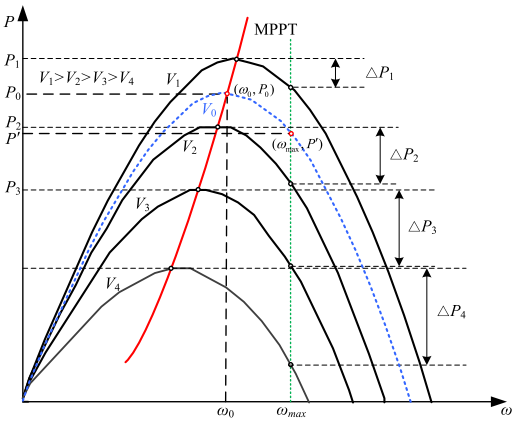

FIGURE 2. The speed-power curve family under different wind speeds.

In (4), K_{df} and K_{pf} are two control coefficients: K_{df} represents the moment of inertia of the WT, and K_{pf} represents the damping coefficient that the WT can provide. Setting the appropriate K_{df} and K_{pf} can effectively improve the dynamic frequency response capability of the WT and provide transient frequency support for the system.

The rotor speed can be quickly adjusted to respond to changes in system frequency in time and provide rotary inertia similar to the synchronous machine; however, the rotor speed depends on the wind speed and operating state and is subject to the rotor speed limit (speed adjustable range is generally 0.7 p.u. to 1.2 p.u.), shortening the duration of the adjustment. This process is also likely to cause a secondary reduction of the frequency in the process of rotor speed recovery.

B. DE-LOADING CONTROL

DLC enables WTs to operate at the secondary power tracking point, leaving the backup to support the system frequency regulation. The DLC method mainly provides over-speed control and pitch control.

As shown in Fig. 1, FA is the MPPT curve; FB is the over-speed operation curve; FC is the deceleration operation curve; and DE_1, DE_2, and DE_3 are the corresponding relationship curves of WT output and speed when the pitch angle is β_1, β_2 and β_3, respectively. As seen in the figure, in MPPT mode, the WT runs at point A, where the output is the maximum output P_{max} at the current wind speed; in the over-speed mode, the WT runs at point B, and in the deceleration mode, the WT runs at point C. Over-speed control and deceleration control can both achieve WT de-loading operation. Over-speed control is more commonly used because of the small interference stability problems brought by deceleration control. Increasing the speed can make the operation curve move to the right and reduce the output, which leaves a certain amount of spare capacity. When the system frequency drops, the WT decelerates, and the operation curve moves to the left, increases the output and inhibits the system frequency reduction. As seen from DE_1, DE_2, and DE_3, a larger pitch angle results in a smaller output. Setting aside a certain pitch angle for power reserve, when the system frequency fluctuates, the frequency deviation is introduced, and the pitch angle changes with the frequency deviation, which adjusts the output of WTs and maintains the system frequency stability.

C. JOINT CONTROL OF RKC AND DLC

RKC can provide inertial support, and DLC can provide system active standby. Combining the advantages of the two strategies can further improve the WT frequency response characteristics. To utilize the kinetic energy in the rotor, the RKC module is introduced into the power control link. On the basis of these conditions, the operating zone of the WT is divided into the over-speed de-loading zone and the pitch de-loading zone: in the over-speed de-loading zone, the RKC and the RSC work together, and in the pitch reduction zone, the RKC and PC work together, thereby achieving the joint control of RKC and DLC.

To give full play to the frequency adjustment potential of WTs, it is necessary to adopt the appropriate method to divide the over-speed de-loading zone and the pitch de-loading zone.

III. PARTITIONING METHOD BASED ON LIMITED OVER-SPEED DE-LOADING CURVE

A. METHOD OF DIVIDING OVER-SPEED DE-LOADING ZONE AND PITCH DE-LOADING ZONE

The DLC mode preferentially uses OSC because of its fast response speed. The method of dividing the de-loading zone and the pitch de-loading zone is based on the application range of over-speed de-loading, that is, the limited over-speed de-loading level.

The relationship of output and speed of the WT at different wind speeds is shown in Fig. 2, in which the red line represents the WT maximum power tracking curve. This figure shows that the de-loading power ΔP under OSC is related not only to the WT speed but also to the wind speed. The maximum de-loading level of the wind speed control is limited by the maximum speed of the WT and will change as

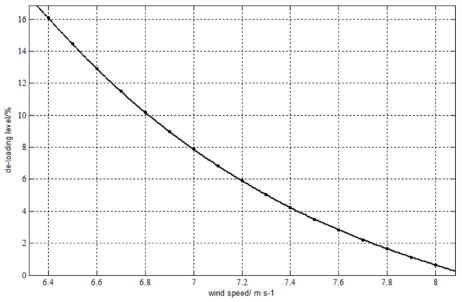

FIGURE 3. Maximum de-loading level by OSC under different wind speeds.

wind speed changes. It can be assumed that the WT reaches the maximum speed after OSC, and the relationship between the OSC maximum de-loading level and the wind speed is deduced reversely under the condition of known output and de-loading level.

The inverse deduction method is used to determine the relationship of the limited over-speed de-loading level and wind speed:

(i) If the de-loading level of the WT is $d\%$, the relationship between the output of the system after the de-loading and the output P before the de-loading is as follows:

$$P' = (1 - d\%)P \tag{5}$$

(ii) Assuming that the speed of the rotor reaches the maximum value $\omega_{\max}$ after the over-speed de-loading, the corresponding output power of the WT is P'. According to the current P' and (5), the power P_0 before de-loading can be obtained, as shown in Fig. 2.

(iii) When the WT does not reach the maximum speed, it runs at the maximum power tracking zone and the pitch angle is 0ř . The corresponding speed ω_0 is obtained according to the maximum power tracking curve of the WT.

(iv) According to the output power (1) of DFIG and the tip speed ratio $\lambda = \omega R/V$, the corresponding V_0 is obtained.

(v) V_0 is the maximum wind speed of the over-speed de-loading under the de-loading level $d\%$.

When the wind speed meets $V_{\min} < V < V_0$, over-speed control can be used to achieve the de-loading level of $d\%$. When the wind speed meets $V_0 < V < V_{\max}$, it cannot achieve the de-loading level of $d\%$ by over-speed control. Therefore, under this de-loading level, $V_{\min} < V < V_0$ is in the over-speed de-loading zone, and V_0 <V< $V_{\max}$ is in the pitch de-loading zone.

Take the DFIG with capacity of 2 MW and a maximum speed of 1.2 p.u. as an example (see Appendix for other relevant parameters). The relationship between the maximum de-loading level and the wind speed that can be achieved by the above method is shown in Fig. 3. The maximum de-loading level wind speed curve of different WTs can be deduced according to the basic operating parameters by the method.

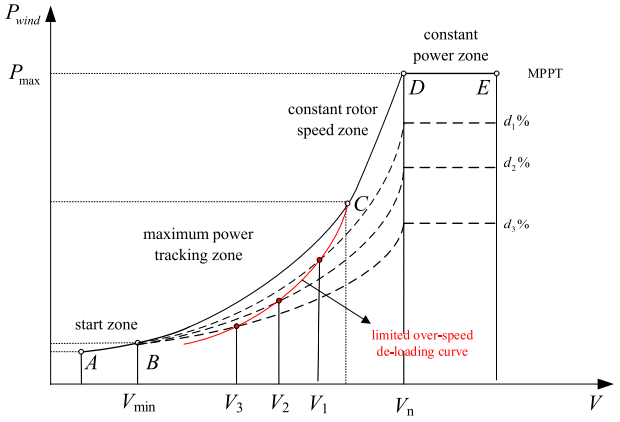

FIGURE 4. The power curve after de-loading.

B. PARTITION CONTROL BASED ON THE LIMITED OVER-SPEED DE-LOADING CURVE

Once the over-speed maximum de-loading level curve is obtained, it is combined with the WT running curve to obtain the demarcation point of the over-speed de-loading zone and the pitch de-loading zone.

Under normal circumstances, the WT operating area is divided into the start zone (AB section), the maximum power tracking zone (BC section), the constant speed zone (CD section) and the constant power zone (DE section), as shown in Fig. 4, which can be obtained according to the WT equipment parameters. If the WT runs under de-loading control, with the improvement of de-loading level, the WT running curve will move down, as shown in the dotted lines in Fig. 4.

The limited overs-peed de-loading curve can be obtained according to the maximum over-speed de-loading level curve of the WT in Fig. 3. The red line intersects with the different de-loading run curves. The intersection point (V_0, P') is the demarcation point of the over-speed de-loading zone and the pitch reduction area at the current de-loading level; that is, at the current de-loading level, when the wind speed meets $V_{\min} < V < V_0$, OSC should be adopted, and when $V_0 < V < V_{\max}$, PC should be adopted.

The absolute amount $|\Delta P|$ of de-loading in the over-speed de-loading zone can be expressed as follows:

$$|\Delta P| = P_0 \times d\% \tag{6}$$

The absolute amount of de-loading is related to not only the level of de-loading but also the output of WT before the de-loading. Considering that the output of WT is affected by wind speed, the situation where the monotonicity of the de-loading level $d\%$ and $|\Delta P|$ is inconsistent may occur. However, because the power under over-speed de-loading control is obtained by $P' = (1 - d\%)P$ and the influence of the output before de-loading is taken into account, the characteristics of the over-speed limited de-loading curve and the judgment mode are not affected.

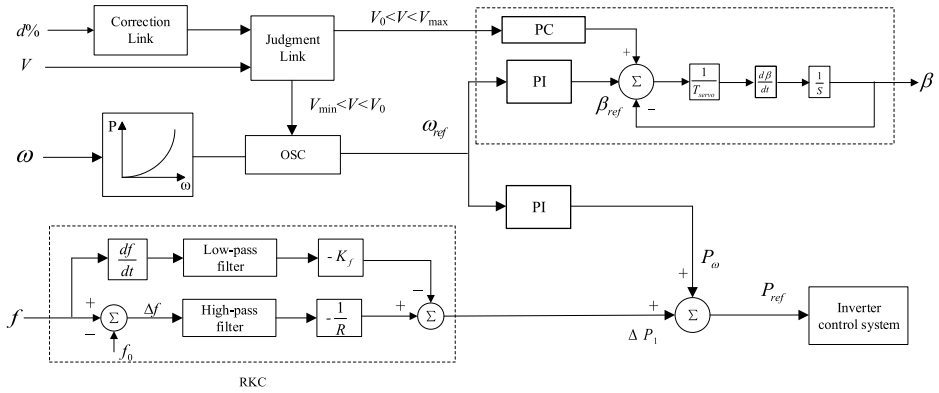

FIGURE 5. Schematic diagram of joint control strategy based on limited over-speed de-loading partitioning.

Fig. 4 shows that the wind speeds of the dividing points corresponding to the de-loading levels $d_1\%$, $d_2\%$ and $d_3\%$ are V_1, V_2 and V_3, respectively. In actual operation, the corresponding demarcation point can be obtained according to the specified de-loading level. Fig. 4 shows that the wind speed of the de-loading level corresponds to the demarcation point.

If a fixed partitioning is set—for example, if the wind speed V_1 is set as the demarcation point—then the over-speed de-loading cannot satisfy the de-loading level $d_3\%$ when the actual wind speed is $V_3 < V < V_1$. If the wind speed V_2 is set as the demarcation point, then the WT operates in the pitch de-loading zone when the actual wind speed is $V_2 < V < V_1$ and the de-loading level is $d_1\%$; however, the over-speed control can also meet the de-loading level $d_1\%$, which cannot take full advantage of over-speed control but instead exacerbates the wear on the WT because of frequent pitch. Theoretically, the control strategy based on the limited over-speed de-loading curve partitioning can effectively take advantage of the various control strategies.

IV. JOINT CONTROL BASED ON THE LIMITED OVER-SPEED DE-LOADING CURVE PARTITIONING

Based on the above control method, the corresponding control link is designed. The block diagram of joint control based on division of over-speeding de-loading limit curve is shown in Fig. 5. Two control links are added to the joint control to improve the control structure.

A. JUDGMENT LINK

The judgment link mainly realizes the partitioning of the over-speed de-loading zone and the pitch de-loading zone. The input is the wind speed V and the de-loading level $d\%$. The demarcation point wind speed V_0 is obtained by the intersection of the over-speeding de-loading limited curve in Section III.B and the de-loading operating power curve. According to this approach, V_0 can be used to make a decision: when $V_{\min} < V < V_0$, OSC is adopted to achieve de-loading operation; when $V_0 < V < V_{\max}$, the PC is adopted to achieve de-loading operation.

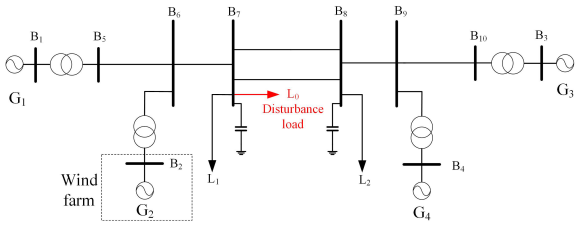

FIGURE 6. Simulation system diagram.

B. CORRECTION LINK

To enable the de-loading capacity of the WT to respond to the change of the system frequency, it is necessary to introduce the correction link into the control to correct the de-loading coefficient and adjust the output of the WT when the load disturbance occurs in the system. The specific de-loading coefficient correction formula is as follows:

$$d'\% = d\%(1 + K\frac{\Delta f}{f_0}) \tag{7}$$

In (7), $d'\%$ is the corrected de-loading level, $d\%$ is the de-loading level before disturbance, K is the correction coefficient, Δf is the frequency deviation, and f_0 is the reference frequency. When the system load disturbance occurs, the de-loading will be adjusted according to the frequency deviation of the system. At the moment, the wind speed or pitch angle will respond to the change of system load.

In the whole frequency adjustment process, RKC provides only inertial support for the system and cannot increase the output of the WT; thus, the primary frequency capacity of WTs is mainly related to de-loading control. The output variation of the WT during the first frequency adjustment process is as follows:

$$\Delta P = -K\frac{\Delta f}{f_0}P_0 \times d\% \tag{8}$$

In (8), the magnitude of the correction coefficient K directly affects the primary frequency adjustment capability of the WT. The magnitude of K is related to the actual output P_0, the rated output P_N, the de-loading level $d\%$ and

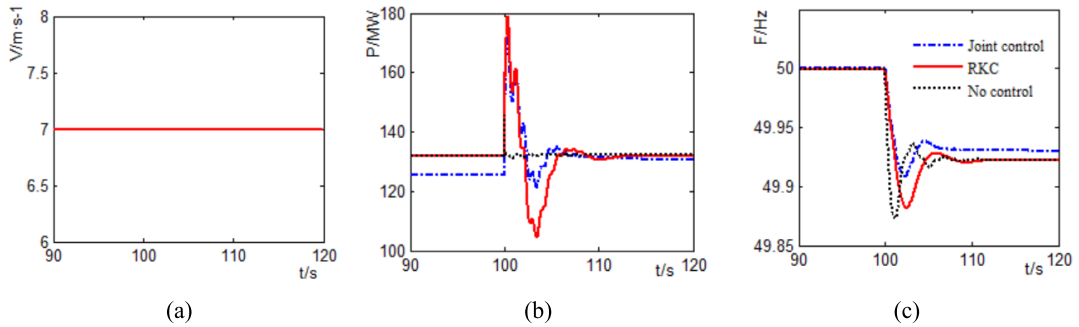

FIGURE 7. The simulation results under wind speed of 7 m/s and de-loading level of 5%. (a) wind speed. (b) output of wind turbine. (c) frequency.

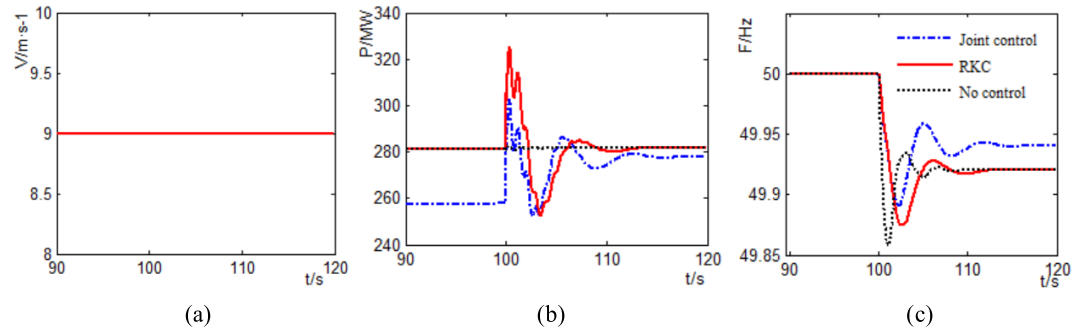

FIGURE 8. The simulation results under wind speed of 9 m/s and de-loading level of 8%. (a) wind speed. (b) output of wind turbine. (c) frequency.

TABLE 1. The time required for frequency stabilization under different control strategies.

Wind speed	No control	RKC	Joint control
7 m/s	12.35	12.23	6.61
9 m/s	12.42	12.38	14.23
11 m/s	12.48	12.41	19.89

other factors. In the simulation experiment, the setting range of K is 2 to 50, which ensures that the WT has a good control effect on the load disturbance.

V. SIMULATION CASE

The simulation is based on the system shown in Fig. 6 [14], [18]. The system contains 10 nodes; the capacities of G_1, G_3, and G_4 are 800 MW, 800 MW, and 1050 MW, respectively; the wind farm is connected to the bus B_6 by transformers; the system loads L_1 and L_2 are 1600 MW and 967 MW, respectively, and L_0 is the disturbance load. The disturbance load is set as 100 MW at 90 s. G_2 is a wind farm containing 250 sets of 2 MW WTs.

A. VERIFICATION OF VALIDITY

The simulation results are shown in Figs. 7-10. The results of wind power penetration rate under 20% are displayed in Figs. 7, 8 and 9. The frequency characteristics of these three cases show the following:

(i) Employing certain control strategies can allow DFIGs to participate in the power system frequency regulation to improve the frequency stability of the system.

(ii) RKC is able to decrease the maximum frequency deviation Δf_{max} caused by disturbance loads, but the effect on the steady-state frequency Δf of the system is very small.

(iii) The joint control can reduce the maximum frequency deviation Δf_{max} of the system and the steady-state frequency deviation Δf.

(iv) The contribution to system frequency stability is as follows: joint control>RKC>no control.

The time required for frequency stabilization under different control strategies is shown in Table 1. RKC contributes little to the time required for system stability. In the low wind speed zone (7 m/s), the joint control uses OSC to participate in the de-loading and the response speed is fast, which accelerates the system stability. In the medium and high wind speed zones (9 m/s and 11 m/s, respectively), PC is used to adjust the frequency in the joint control, which requires a longer time, but the system changes less in the latter part of the adjustment process.

For example, when the wind speed is 9 m/s, and the de-loading level is 8%, the frequency difference is shown in Table 2. Compared to RKC, the Δf_{max} is reduced by 0.01625 Hz under joint control, and the Δf is reduced by 0.02015 Hz. The frequency of the system under different penetration and control methods with 20% de-loading is shown in Fig. 10 clearly shows the proposed joint control

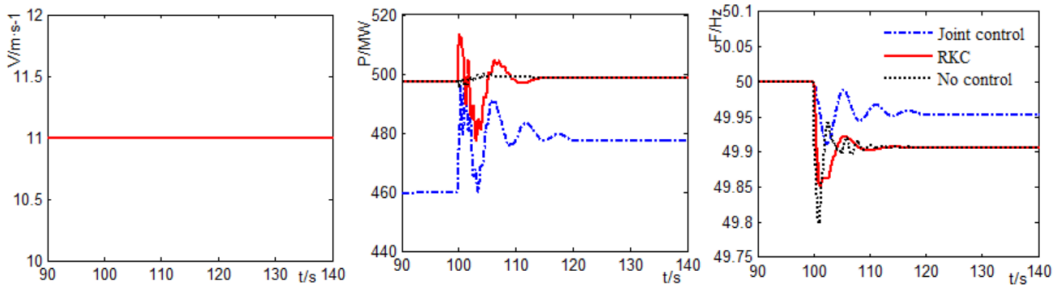

FIGURE 9. The simulation results under wind speed of 11 m/s and de-loading level of 10%. (a) wind speed. (b) output of wind turbine. (c) frequency.

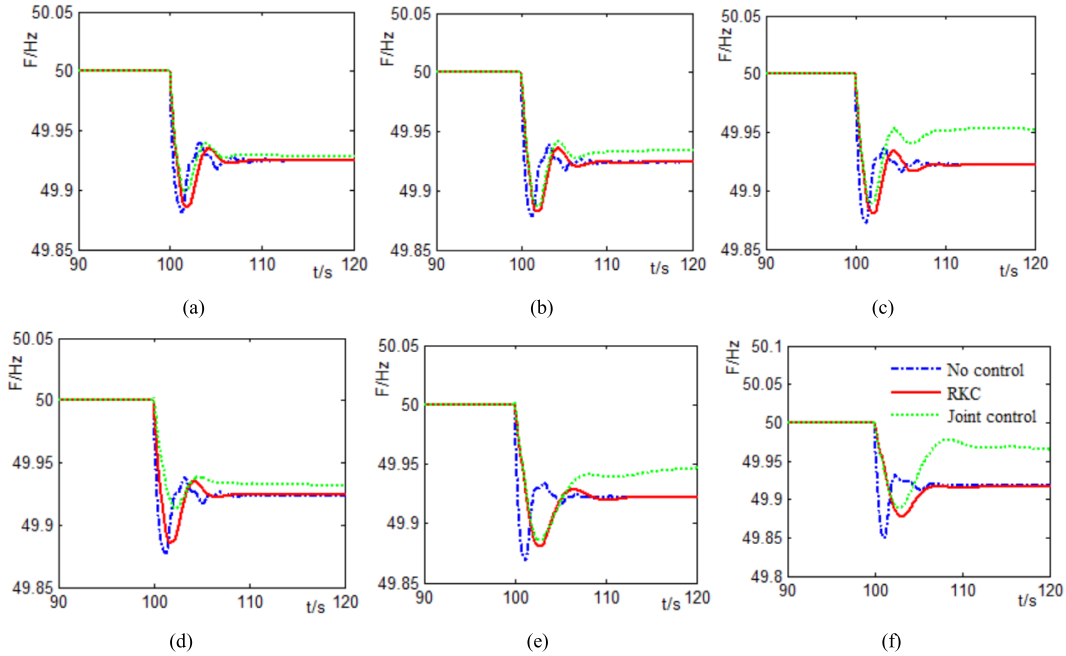

FIGURE 10. Frequency change of the system under different penetration and control modes. (a) penetration 10%, wind speed 7 m/s. (b) penetration 10%, wind speed 9 m/s. (c) penetration 10%, wind speed 11 m/s. (d) penetration 30%, wind speed 7 m/s. (e) penetration 30%, wind speed 9 m/s. (f) penetration 30%, wind speed 11 m/s.

TABLE 2. The simulation results under a wind speed of 9 m/s and de-loading level of 8%.

Control method	No control	RKC	Joint control
Maximum frequency deviation/Hz	0.14154	0.12563	0.10938
Steady-state frequency deviation/Hz	0.07987	0.07980	0.05965

strategy has a better control effect and adapts to different wind conditions. The simulation results verify the validity and rationality of the proposed control strategy.

B. COMPARISON BETWEEN THE LIMITED OVER-SPEED DE-LOADING CURVE PARTITIONING AND THE FIXED PARTITIONING

The proposed joint control is based on the over-speed limited de-loading curve partitioning, which is a variable partitioning method. From the speed of the WT in Fig. 11 (b), it can be understood that when the wind speed is 7.5 m/s with a de-loading level of 3%, if the variable is adopted, the WT operates in the over-speed de-loading zone and uses OSC to achieve de-loading; however, if the fixed partitioning is adopted, pitch control will be chosen to achieve de-loading. From the frequency characteristics, it can be seen that compared to the fixed partitioning, the changeable partitioning will not only raise the lowest point of the frequency but also make the system tend to stabilize faster because it takes full advantage of the rapid response characteristics of OSC. When the rotor speed increases, the available rotor kinetic energy will be greater, increasing the system of inertia, which makes

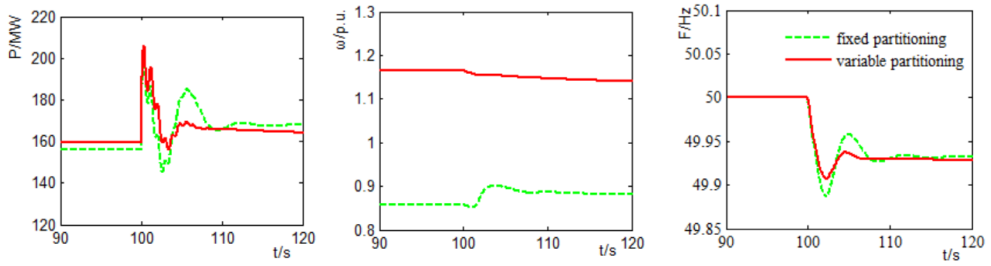

FIGURE 11. The simulation results of fixed partitioning and variable partitioning based on limited over-speed de-loading curve under a wind speed of 7.5 m/s and de-loading level of 3%. (a) output of wind turbine. (b) rotor speed. (c) frequency.

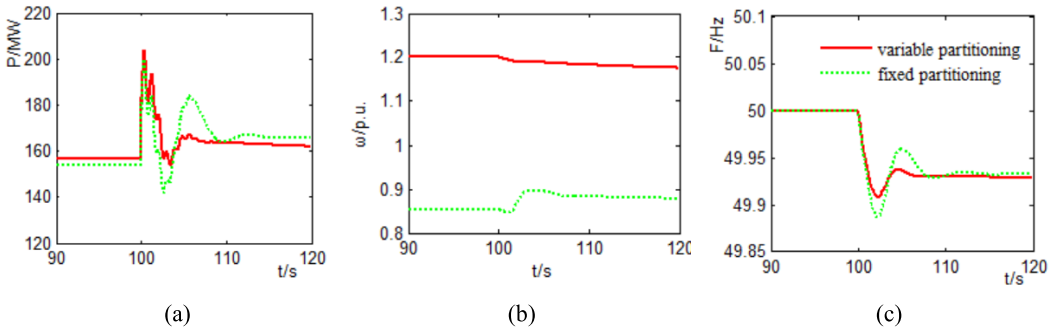

FIGURE 12. The simulation results of fixed partitioning and variable partitioning based on limited over-speed de-loading curve under a wind speed of 7.5 m/s and de-loading level of 4.5%. (a) output of wind turbine. (b) rotor speed. (c) frequency.

TABLE 3. The changes in wind farm 1 output under a wind speed of 7 m/s and a de-loading level of 10%.

Control method	No control	RKC	Joint control
Active power before load disturbance /MW	79.265	79.265	71.455
Active power before load disturbance /MW	79.265	79.002	79.263

TABLE 4. The changes in wind farm 2 output under a wind speed of 7 m/s and a de-loading level of 10%.

Control method	No control	RKC	Joint control
Active power before load disturbance /MW	79.265	79.265	71.354
Active power before load disturbance /MW	79.265	79.008	79.259

the WT at this time exhibit good dynamic frequency response characteristics.

As shown in Fig. 12, under the de-loading level of 4.5%, the WT rotor speed reached the maximum 1.2 p.u. by the changeable partitioning, i.e., the proposed control strategy is still superior to the fixed partitioning approach. It can be observed from Fig. 13 that although the dynamic response characteristics of the system frequency with the fixed partitioning approach are better than that with the proposed approach, the speed of the WT in the former method has exceeded the maximum value, causing the WT work to fail and showing that the fixed method is not feasible.

C. ANALYSIS OF THE COMPARISON BETWEEN CONTROL METHODS OF SWITCHING THE OPERATION MODE OF THE WIND TURBINE

The simulation of SOM control in [17] is compared and analyzed with that of the joint control strategy proposed in this paper. The simulation results are shown in Fig. 14. In the low wind speed zone, the wind speed is 6.8 m/s; in the medium wind speed zone, the wind speed is 10 m/s; and in the high wind speed zone, the wind speed is 13 m/s.

Fig. 14 shows that in the low wind speed zone, the joint control significantly reduces the maximum frequency deviation and steady-state frequency deviation of the system

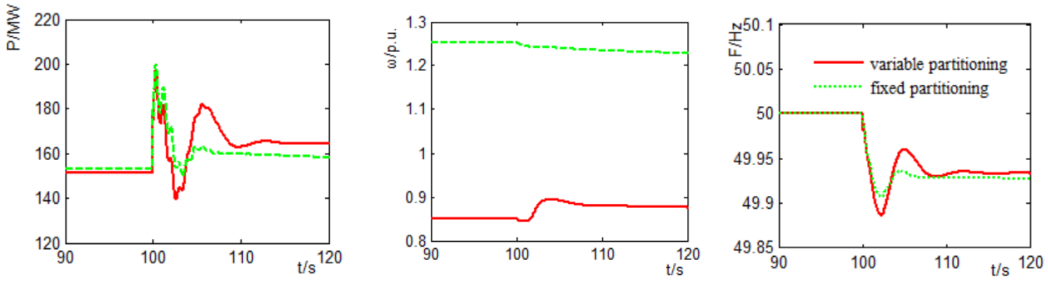

FIGURE 13. The simulation results of fixed partitioning and variable partitioning based on limited over-speed de-loading curve under a wind speed of 7.5 m/s and de-loading level of 6%. (a) output of wind turbine. (b) rotor speed. (c) frequency.

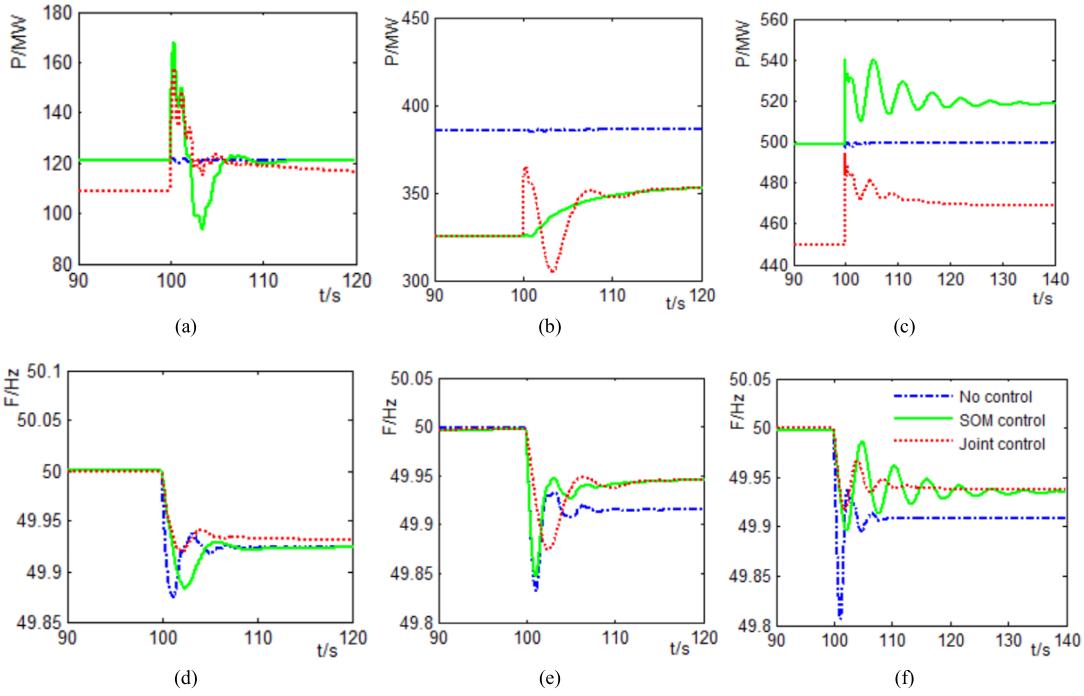

FIGURE 14. The results of a comparison between the switching operation mode control method. (a) output of WT at the speed of 6.8 m/s. (b) output of WT at the speed of 10 m/s. (c) output of WT at the speed of 13 m/s. (d) frequency of system at the speed of 6.8 m/s. (e) frequency of system at the speed of 10 m/s. (f) frequency of system at the speed of 13 m/s

TABLE 5. The changes in system frequency under a wind speed of 7 m/s and a de-loading level of 10%.

Control method	No control	RKC	Joint control
Maximum frequency deviation /Hz	0.17103	0.15821	0.13001
The time for frequency to reach the lowest point /s	9.27	9.68	7.43
Steady-state frequency deviation /Hz	0.12916	0.13096	0.10181
The time required for frequency stabilization /s	28.07	28.15	23.41

compared with the SOM control. In the low wind speed zone, the switching mode control adopts the RKC to realize the short-time overproduction, and the WT that has resumed the speed after stabilization cannot increase the extra output. The joint control uses both the RKC and the over-speed de-loading control. On the one hand, the over-speed de-loading raises the rotor kinetic energy of the WT and reduces the maximum frequency deviation; on the other hand, the de-loading operation leaves the active standby and can increase the steady-state frequency.

In the medium wind speed zone, both control methods adopt the PC to achieve the de-loading operation of

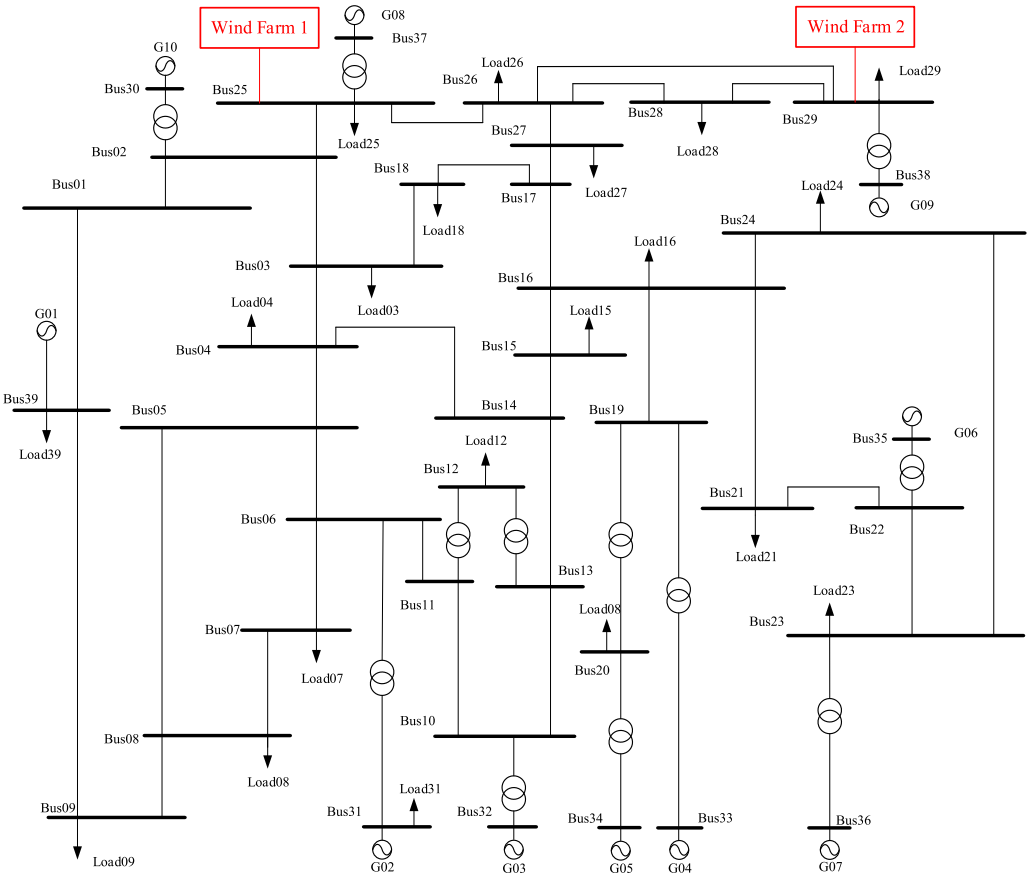

FIGURE 15. Single line diagram of the 39 Bus New England System

TABLE 6. The changes in wind farm 1 output under a wind speed of 9 m/s and a de-loading level of 10%.

Control method	No control	RKC	Joint control
Active power before load disturbance /MW	169.06	169.06	154.25
Active power before load disturbance /MW	169.11	168.85	166.22

TABLE 7. The changes in wind farm 2 output under a wind speed of 9 m/s and a de-loading level of 10%.

Control method	No control	RKC	Joint control
Active power before load disturbance /MW	169.03	169.03	154.28
Active power before load disturbance /MW	169.06	168.89	166.77

TABLE 8. The changes in system frequency under a wind speed of 9 m/s and a de-loading level of 10%.

Control method	No control	RKC	Joint control
Maximum frequency deviation /Hz	0.16497	0.15002	0.12403
The time for frequency to reach the lowest point /s	9.26	9.63	7.02
Steady-state frequency deviation /Hz	0.12701	0.12800	0.09004
The time required for frequency stabilization /s	28.32	28.46	24.02

the WT; thus, they have similar steady-state frequency curves, as shown in Fig. 14 (b) and Fig. 14 (e). However, in SOM control, the rotating speed of the WT is fixed to the maximum, which cannot respond to the system frequency changes in time, and the lowest point of the frequency changes only slightly. Although the joint control causes the output of the

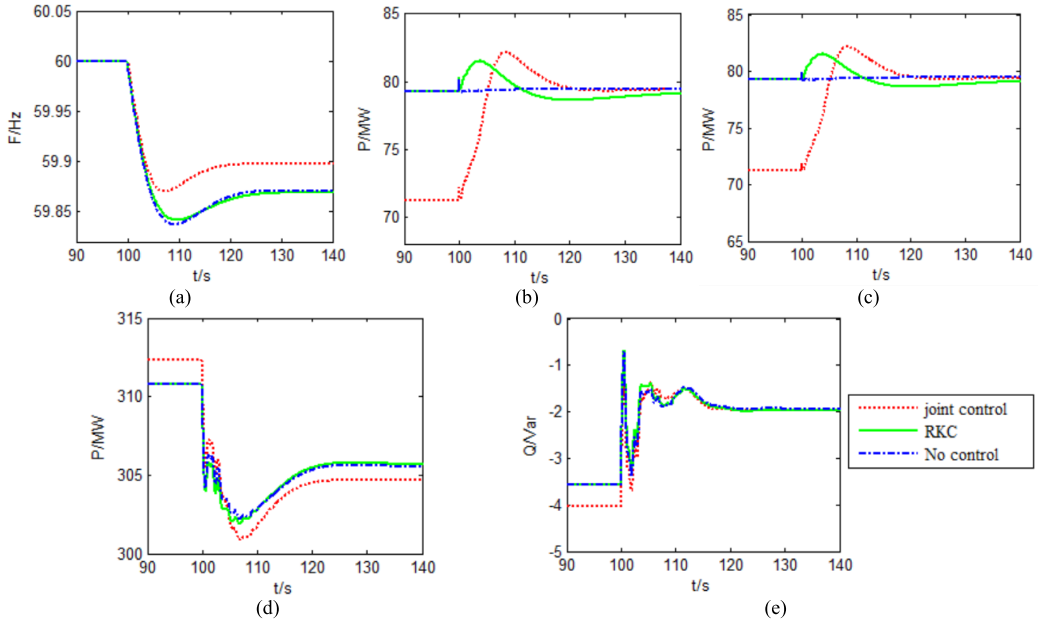

FIGURE 16. System response after load disturbances under a wind speed of 7 m/s and a de-loading level of 10%. (a) frequency. (b) output of wind farm 1. (c) output of wind farm 2. (d) active power of connection line between the two wind farms. (e) reactive power of connection line between the two wind farms.

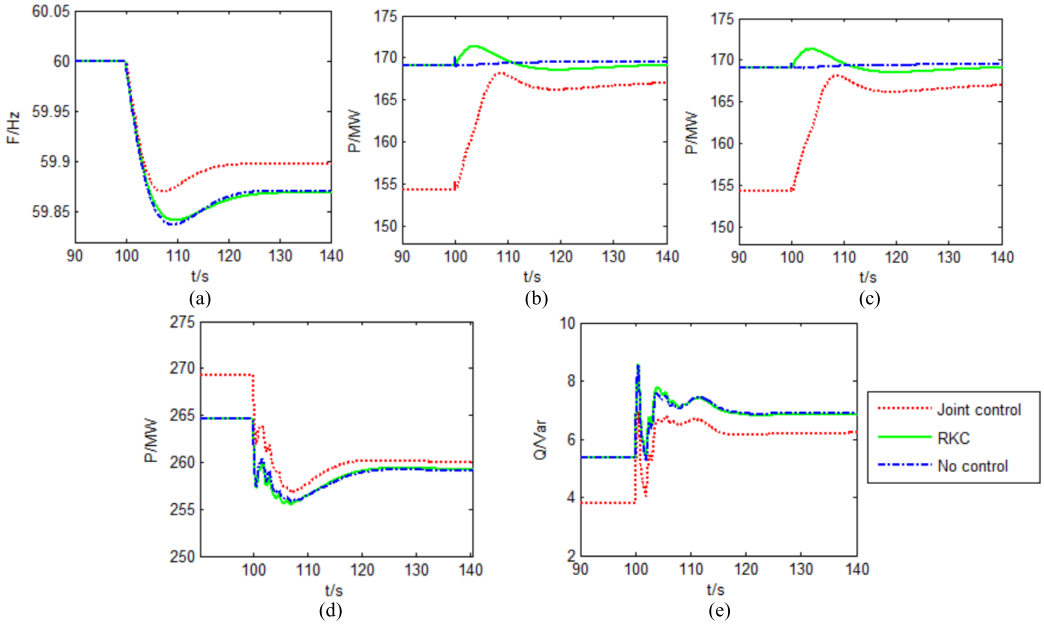

FIGURE 17. System response after load disturbances under a wind speed of 9 m/s and a de-loading level of 10%. (a) frequency. (b) output of wind farm 1. (c) output of wind farm 2. (d) active power of connection line between the two wind farms. (e) reactive power of connection line between the two wind farms.

WT in the frequency adjustment process to produce the phenomenon of short-term fluctuations, the rotating speed of the WT can respond to the system frequency changes in time, which raises the lowest point of the system frequency.

In the high wind speed zone, two types of control strategies can provide similar control effect, and both can improve the system frequency stability. The SOM control enables the WT to generate power through PC; that is, overload operation supports the system frequency, which is bound to increase the capacity of the converter and transformer. As shown in Fig. 14 (c), the output of the WT is increased by approximately 20 MW, but 40 MW is achieved during the process of transient frequency regulation, which further improves the requirements of the grid-connected inverter and

TABLE 9. The changes in wind farm 1 output under a wind speed of 11 m/s and a de-loading level of 10%.

Control method	No control	RKC	Joint control
Active power before load disturbance /MW	299.24	299.24	271.04
Active power before load disturbance /MW	299.35	299.03	287.41

TABLE 10. The Changes in Wind Farm 2 Output under A Wind Speed of 11 m/s And A De-loading Level of 10%.

Control method	No control	RKC	Joint control
Active power before load disturbance /MW	299.17	299.17	154.28
Active power before load disturbance /MW	299.48	299.36	287.33

TABLE 11. The changes in system frequency under a wind speed of 11 m/s and a de-loading level of 10%.

Control method	No control	RKC	Joint control
Maximum frequency deviation /Hz	0.16760	0.15600	0.10102
The time for frequency to reach the lowest point /s	9.04	9.66	5.43
Steady-state frequency deviation /Hz	0.12701	0.12700	0.08303
The time required for frequency stabilization /s	29.72	30.85	18.43

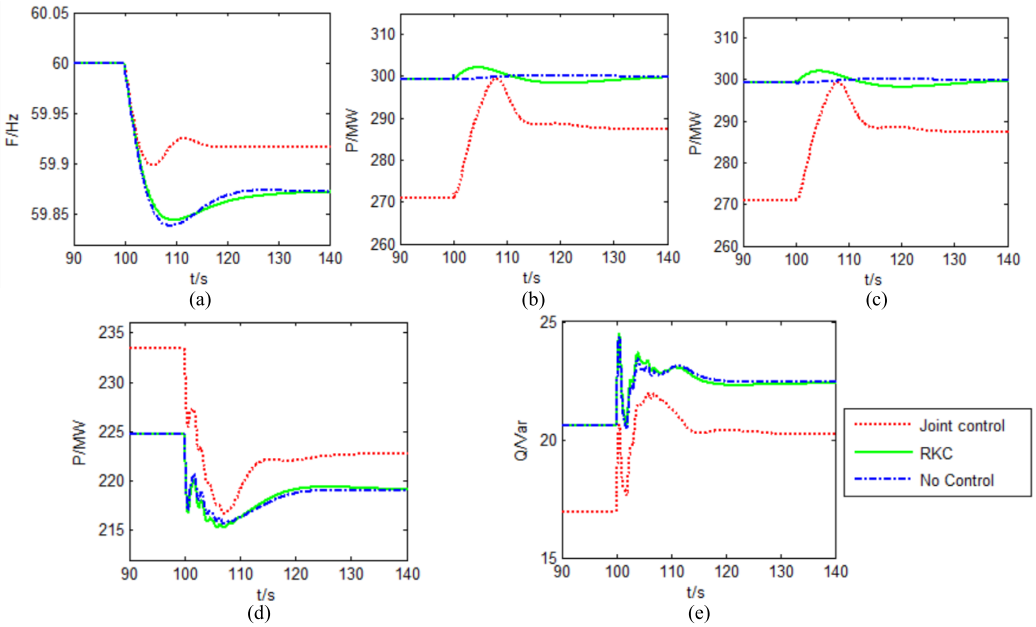

FIGURE 18. System response after load disturbances under a wind speed of 11 m/s and a de-loading level of 10%. (a) frequency. (b) output of wind farm 1. (c) output of wind farm 2. (d) active power of connection line between the two wind farms. (e) reactive power of connection line between the two wind farms.

transformer and is not conducive to the economic operation of the large-scale wind power grid. The contrasting simulation further illustrates the advantages of the proposed control strategy.

D. ADDITIONAL SIMULATION IN IEEE-39 BUS NEW ENGLAND SYSTEM

To prove the generality of the proposed control strategy, a simulation on an IEEE-39 Bus New England System shown in Fig. 15 is added. Two 300 MW wind farms are incorporated at bus 25 and bus 29. The load suddenly increases by 100 MW at bus 9 in 100 s. The simulation verifies the effectiveness of the proposed joint control strategy under different wind speed conditions. The simulation parameters can be found on the website http://www.sel.eesc.usp.br/ieee/IEEE39/.

The results in Fig. 16 to Fig. 18 and Table 3 to Table 11 show that the proposed control strategy has the same effect in the IEEE-39 bus system as that in the

four-machine two-zone system and further verifies the validity and rationality of the proposed control. From the system frequency characteristics and the active and reactive power lines of the two wind farms, there is no permanent oscillation in the system, which indicates that the proposed control strategy is practical.

VI. CONCLUSION

In this paper, the frequency regulation capabilities of OSC and PC were analyzed theoretically, the applicable range of over-speed control was quantized, and the limited over-speed de-loading curve was deduced and fitted. A wind power frequency regulation control strategy based on limited over-speed de-loading curve partitioning was proposed. The following conclusions were obtained through theoretical analysis and simulation:

(i) The limited over-speed de-loading level is closely related to the operating state of the WT. The greater the wind speed is, the smaller the over-speed limit de-loading level will be.

(ii) The maximum de-loading level of the WT was deduced using the "reverse derivation method," and it was fitted to provide the basis for the partitioning of the over-speed de-loading zone and the pitch de-loading zone.

(iii) The frequency regulation control strategy based on limited over-speed de-loading curve partitioning realizes the partition control for the de-loading level, which makes full use of the advantages of over-speed de-loading and exploits the frequency regulation capability of the WT itself. The simulation results showed that the proposed strategy can effectively improve the inertia of the system and the frequency stability under complex operating conditions.

(iv) In this paper, the influence of instantaneous fluctuation of wind speed was neglected. The frequent swing of the wind speed near the demarcation point may cause frequent switching of the WT, which is not conducive to the stable control of the WT. Combined with the short-term fluctuations of wind speed, the next step is to further improve the control method proposed.

(v) The proposed control method can improve the frequency response capacity of WTs, provide effective frequency support for a power system according to the de-loading operation requirement by dispatchers and enhance the wind power acceptance capacity of the system. However, because of the complicated operating conditions of WTs and multiple factors influencing frequency regulation control, further study is required to assess the frequency regulation capacity of wind power to reduce the conventional units of standby of the system and balance the economic contradictions between the maximum output of WTs and de-loading frequency regulation.

APPENDIX

DFIG-related parameters: the starting speed of the WT is 0.51 p.u., the maximum speed is 1.2 p.u., the removal wind speed is 21 m/s, and the rated wind speed 11 m/s. Start zone: 5.1 m/s to 6.3 m/s; maximum power tracking zone: 6.3 m/s to 10.3 m/s; constant speed zone: 10.3 m/s to 11 /s; and constant power zone: 11 m/s to 21 m/s. The power curve during the WT operation is shown in Fig. 19.

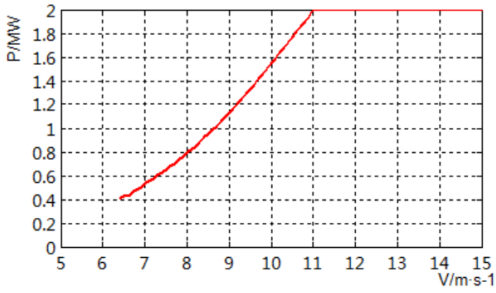

FIGURE 19. The power curve of a wind turbine.

REFERENCES

[1] M. Dreidy, H. Mokhlis, and S. Mekhilef, "Inertia response and frequency control techniques for renewable energy sources: A review," *Renew. Sustain. Energy Rev.*, vol. 69, pp. 144–155, Mar. 2017.
[2] V. Y. Singarao and V. S. Rao, "Frequency responsive services by wind generation resources in United States," *Renew. Sustain. Energy Rev.*, vol. 55, pp. 1097–1108, Mar. 2016.
[3] J. Morren, S. W. H. de Haan, W. L. Kling, and J. A. Ferreira, "Wind turbines emulating inertia and supporting primary frequency control," *IEEE Trans. Power Syst.*, vol. 21, no. 1, pp. 433–434, Feb. 2006.
[4] Q. Shi, G. Wang, and W. Ma, "An experimental study method of D-PMSG with virtual inertia control," *Proc. CSEE*, vol. 35, no. 8, pp. 1292–1306, 2015.
[5] S. D. Rijcke, P. Tielens, B. Rawn, D. V. Hertem, and J. Driesen, "Trading energy yield for frequency regulation: Optimal control of kinetic energy in wind farms," *IEEE Trans. Power Syst.*, vol. 30, no. 5, pp. 2469–2478, Sep. 2015.
[6] Q. Shi, G. Wang, W. Ma, L. Fu, Y. Wu, and P. Xing, "Coordinated virtual inertia control strategy for D-PMSG considering frequency regulation ability," *J. Elect. Eng. Technol.*, vol. 11, pp. 1921–1935, Nov. 2016.
[7] J. Lee, E. Muljadi, P. Srensen, and Y. C. Kang, "Releasable kinetic energy-based inertial control of a DFIG wind power plant," *IEEE Trans. Sustain. Energy*, vol. 7, no. 1, pp. 279–288, Jan. 2015.
[8] R. G. de Almeida, E. D. Castronuovo, and J. A. P. Lopes, "Optimum generation control in wind parks when carrying out system operator requests," *IEEE Trans. Power Syst.*, vol. 21, no. 2, pp. 718–725, May 2006.
[9] K. V. Vidyanandan and N. Senroy, "Primary frequency regulation by deloaded wind turbines using variable droop," *IEEE Trans. Power Syst.*, vol. 28, no. 2, pp. 837–846, May 2013.
[10] J. Tan and Y. Zhang, "Coordinated control strategy of a battery energy storage system to support a wind power plant providing multi-timescale frequency ancillary services," *IEEE Trans. Sustain. Energy*, vol. 8, no. 3, pp. 1140–1153, Jul. 2017.
[11] K. V. Vidyanandan and N. Senroy, "Frequency regulation in a wind–diesel powered microgrid using flywheels and fuel cells," *IET Generat. Transmiss. Distrib.*, vol. 10, no. 3, pp. 780–788, 2016.
[12] J. W. Choi, S. Y. Heo, and M. K. Kim, "Hybrid operation strategy of wind energy storage system for power grid frequency regulation," *IET Generat. Transmiss. Distrib.*, vol. 10, no. 3, pp. 736–749, 2016.
[13] Z. Zhang, Y. Z. Sun, G. J. Li, L. Cheng, and J. Lin, "Frequency regulation by doubly fed induction generator wind turbines based on coordinated overspeed control and pitch control," *Autom. Electr. Power Syst.*, vol. 35, no. 17, pp. 20–25, 2011.
[14] L. Ding, S. Yin, and T. X. Wang, "Integrated frequency control strategy of dfigs based on virtual inertia and over-speed control," *Power Syst. Technol.*, vol. 39, no. 9, pp. 2385–2391, 2015.
[15] J. Zhao, X. Lv, Y. Fu, and X. Hu, "Frequency regulation of the wind/photovoltaic/diesel microgrid based on DFIG cooperative strategy with variable coefficients betweenvirtual inertia and over-speed control," *Trans. China Electrotech. Soc.*, vol. 30, no. 5, pp. 59–68, 2015.

[16] S. Ghosh, S. Kamalasadan, N. Senroy, and J. Enslin, "Doubly fed induction generator (DFIG)-based wind farm control framework for primary frequency and inertial response application," *IEEE Trans. Power Syst.*, vol. 31, no. 3, pp. 1861–1871, May 2016.
[17] A. B. Attya and T. Hartkopf, "Wind turbine contribution in frequency drop mitigation—Modified operation and estimating released supportive energy," *IET Generat. Transmiss. Distrib.*, vol. 8, no. 5, pp. 862–872, 2014.
[18] J. M. Mauricio, A. Marano, A. Gómez-Expósito, and J. L. M. Ramos, "Frequency regulation contribution through variable-speed wind energy conversion systems," *IEEE Trans. Power Syst.*, vol. 24, no. 1, pp. 173–180, Feb. 2009.

XU ZHANG (M'11) was born in Shanxi, China, in 1975. He received the B.S. degree from the Taiyuan University of Technology and the M.S. and Ph.D. degrees in power systems and automation from North China Electric Power University, Beijing, China, in 2005 and 2013, respectively.

He is currently an Assistant Professor with the School of Electrical and Electronic Engineering, where he has been since 2005. His current research interests include the area of power system intelligent analysis and control, power system frequency regulation by wind power, power grid fault diagnosis and restoration, and NP problems in power system online analytics.

XIAOBING ZHA (S'16) was born in Anhui, China, in 1992. He received the B.S. degree in biological engineering from Chongqing University and the M.S. degree in power systems and automation from North China Electric Power University, Beijing, China, in 2018. His research interests include power system frequency regulation by wind power.

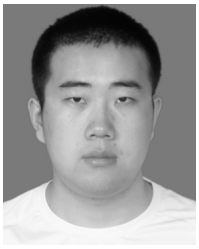

SHUAI YUE (S'16) received the B.S. degree from the Shenyang University of Technology, Shenyang, China, in 2016. He is currently pursuing the M.S. degree in electrical engineering from North China Electric Power University, Beijing, China. His research interests include the area of power grid fault diagnosis and wind farm modeling.

YUNLONG CHEN received the B.S. degree from the China University of Mining and Technology, Beijing, China, in 2017. He is currently pursuing the M.S. degree in power system and automation from North China Electric Power University, Beijing. His research interests include the area of wind power frequency regulation capacity assessment.